INTERNATIONAL JOURNAL FOR NUMERICAL METHODS IN FLUIDS, VOL. 23, 77–103 (1996)

MODELLING AND NUMERICAL SIMULATION OF LOW-MACH-NUMBER COMPRESSIBLE FLOWS

CHIN-HSIEN LI

CSIRO Division of Mathematics and Statistics, Locked Bag 17, North Ryde, N.S.W. 2113, Australia

ROLAND GLOWINSKI

University of Houston, Houston, TX, U.S.A.

SUMMARY

Based upon the operator-splitting method designed by the authors to solve the Navier–Stokes equations with variable density and viscosity, a segregated time-marching solution scheme is proposed for solving the low-Mach-number flow model with the acoustic waves being filtered out. This solution scheme does not rely on the correction for global mass conservation to maintain solution accuracy. With this advantage the scheme can be directly applied to general low-Mach-number flow problems with confidence.The scheme is validated by comparing the results for a number of test cases with known limiting exact solutions and published numerical solutions by other authors.

KEY WORDS: operator splitting; low-Mach-number flows; natural convection

1. INTRODUCTION

Low-Mach-number compressible flows have a wide range of industrial applications, e.g. combustions, chemical reactions, natural convections. The numerical simulation of low-Mach-number flows is still a challenge to contemporary compressible flow algorithms. As is well known,[1–4] time-marching compressible flow schemes become ineffective at low Mach numbers because of the wide disparity of time scales associated with convection and the rapid propagation of acoustic waves (or disturbances) which quickly contaminates the solutions and therefore reduces the stability of the scheme and destroys the convergence to steady state.

In order to improve convergence and stability, one common approach is to use a modified compressible flow model (called the L-model in this paper) for the low-Mach-number case,[3,5] which excludes acoustic waves by separating the pressure p into a thermodynamic part p_T which is spatially uniform and a hydrodynamic part p_d, with $p_d \ll p_T$ in the low-Mach-number case. The usual variable density model (called the V-model in this paper) and Boussinesq model (called the B-model in this paper) are particular cases of the L-model.

The main purpose of this paper is to present a segregated time-marching solution algorithm for numerical solution of this modified model for low-Mach-number flows. This solution scheme does not rely on the correction for global mass conservation to maintain solution accuracy. With this advantage the scheme can be directly applied to general low-Mach-number flow problems with confidence, especially where such a correction is either impossible or unfeasible. The core of this algorithm is an

CCC 0271–2091/96/020077–27

Received 24 May 1994
Revised 9 October 1995

operator-splitting method designed by the authors for solving the Navier–Stokes equations with variable density and viscosity. The operator-splitting method is an efficient and robust method for solving the Navier–Stokes equations,[8–12] which enables us to decouple the difficulties in solving the Navier–Stokes equations, i.e. continuity constraints, non-linearity, coupling of velocity components, and the resulting subproblems can be solved by specially designed efficient solvers, e.g. a preconditioned conjugate gradient iterative solver.

In Sections 2–4 we present the model equations. In Section 5 we describe the segregated time-stepping scheme. In Section 6 we describe in detail the operator-splitting method for solving the Navier–Stokes equations with variable density and viscosity. In Section 7 we present the results of some numerical tests and comparisons with known limiting exact solutions and published nunmerical solutions by other authors. These results clearly show the validity of our algorithm. The problem of global mass conservation is briefly discussed in Section 8. A rigorous numerical analysis of the algorithm or a systematic numerical study of low-Mach-number flow regimes like the one done by Chenoweth and Paolucci[5] is not the aim of this paper but will be the topic of future papers by the authors.

2. GOVERNING EQUATIONS FOR LOW-MACH-NUMBER COMPRESSIBLE FLOWS

In the low-Mach-number case the dissipation effect in the heat equation may be neglected. Consider the flow in N-dimensional space; assume the vertical (x_3) axis pointing upward. Suppose the only body force is gravity. Then we have the following governing equations.

Continuity equation

$$\frac{\mathrm{D}\rho}{\mathrm{D}t} + \rho\nabla\cdot\mathbf{u} = 0. \tag{1}$$

Momentum equation

$$\rho\frac{\mathrm{D}u_i}{\mathrm{D}t} - \sum_{j=1}^{N}\frac{\partial}{\partial x_j}(2\mu e_{ij} - \tfrac{2}{3}\mu\Lambda\delta_{ij}) + \frac{\partial p}{\partial x_i} = -\rho g n_i, \quad i = 1,\ldots,N, \tag{2}$$

where

$$2e_{ij} = \frac{\partial u_i}{\partial x_j} + \frac{\partial u_j}{\partial x_i}, \qquad \Lambda = \sum_{i=1}^{N}\frac{\partial u_i}{\partial x_i} = \nabla\cdot\mathbf{u},$$

δ_{ij} is the Kronecker delta function and $n_i = \delta_{i3}$.

Heat equation

$$\rho C_{\mathrm{p}}\frac{\mathrm{D}T}{\mathrm{D}t} - \frac{\mathrm{D}p}{\mathrm{D}t} = \sum_{j=1}^{N}\frac{\partial}{\partial x_j}\left(k\frac{\partial T}{\partial x_j}\right) + Q. \tag{3}$$

Equation of state

$$p = R\rho T. \tag{4}$$

Remark 1

In general the conductivity k and viscosity μ are functions of temperature T. In this paper we assume they are of the Sutherland law forms.[5,6] For simplicity, in this paper we assume C_{p} is constant.

Remark 2

From equation (4) we have

$$\frac{1}{\rho}\frac{\mathrm{D}\rho}{\mathrm{D}t}=-\frac{1}{T}\frac{\mathrm{D}T}{\mathrm{D}t}+\frac{1}{p}\frac{\mathrm{D}p}{\mathrm{D}t}. \tag{5}$$

Combined with (1), it yields

$$\frac{\mathrm{D}p}{\mathrm{D}t}+p\boldsymbol{\nabla}\cdot\mathbf{u}=R\rho\frac{\mathrm{D}T}{\mathrm{D}t}. \tag{6}$$

3. MODIFIED EQUATIONS FOR LOW-MACH-NUMBER COMPRESSIBLE FLOWS

In the case of low-Mach-number flows the pressur p may be separated into a thermodynamic part p_{T} which is spatially uniform and a hydrodynamic part p_{d}, with $p_{\mathrm{d}} \ll p_{\mathrm{T}}$:[3,5]

$$p(t;\mathbf{x})=p_{\mathrm{T}}(t)+p_{\mathrm{d}}(t;\mathbf{x}). \tag{7}$$

Also, the equation of state (4) may be approximated by

$$p_{\mathrm{T}}=R\rho T \tag{8}$$

and $\mathrm{D}p/\mathrm{D}t$ by $\mathrm{d}p_{\mathrm{T}}/\mathrm{d}t$ in equations (3) and (6).

By integrating (6) over the flow domain $\Omega\in\mathbb{R}^N$, we obtain an ODE for p_{T}:

$$meas(\Omega)\frac{\mathrm{d}p_{\mathrm{T}}}{\mathrm{d}t}+\left(\int_{\Omega}\boldsymbol{\nabla}\cdot\mathbf{u}\,\mathrm{d}\mathbf{x}\right)p_{\mathrm{T}}=R\int_{\Omega}\rho\frac{\mathrm{D}T}{\mathrm{D}t}\,\mathrm{d}\mathbf{x}, \tag{9}$$

where $meas(\Omega)$ is the volume of the flow domain Ω.

In summary, we arrive at the following modified model (L-model) for low-Mach-number flows.

Continuity equation

$$\frac{\mathrm{D}\rho}{\mathrm{D}t}+\rho\boldsymbol{\nabla}\cdot\mathbf{u}=0. \tag{10}$$

Momentum equation

$$\rho\frac{\mathrm{D}u_i}{\mathrm{D}t}-\sum_{j=1}^{N}\frac{\partial}{\partial x_j}\left(2\mu e_{ij}-\tfrac{2}{3}\mu\Lambda\delta_{ij}\right)+\frac{\partial p_{\mathrm{d}}}{\partial x_i}=-\rho g n_i,\quad i=1,\dots,N. \tag{11}$$

Heat equation

$$\rho C_{\mathrm{p}}\frac{\mathrm{D}T}{\mathrm{D}t}-\sum_{j=1}^{N}\frac{\partial}{\partial x_j}\left(k\frac{\partial T}{\partial x_j}\right)=\frac{\mathrm{d}p_{\mathrm{T}}}{\mathrm{d}t}+Q. \tag{12}$$

Equation of state

$$p_{\mathrm{T}}=R\rho T. \tag{13}$$

ODE for p_T

$$meas(\Omega)\frac{\mathrm{d}p_{\mathrm{T}}}{\mathrm{d}t}+\left(\int_{\Omega}\boldsymbol{\nabla}\cdot\mathbf{u}\,\mathrm{d}\mathbf{x}\right)p_{\mathrm{T}}=R\int_{\Omega}\rho\frac{\mathrm{D}T}{\mathrm{D}t}\,\mathrm{d}\mathbf{x}. \tag{14}$$

Remark 3

Since the dynamic pressure p_d in the momentum equation is now not related to the density variation, this model does not contain acoustic waves.

Remark 4

Let ρ_r be a representative density. Introduce ϕ s.t. $\nabla\phi$ is a unit vector in the direction opposite to gravity and introduce also

$$p_d^* = p_d + \rho_r g\phi + \tfrac{2}{3}\mu\Lambda.$$

Then, rewriting p_d^* as p_d, the momentum equation (11) can be rewritten as

$$\rho\frac{\mathrm{D}u_i}{\mathrm{D}t} - \sum_{j=1}^{N}\frac{\partial}{\partial x_j}\left[\mu\left(\frac{\partial u_i}{\partial x_j} + \frac{\partial u_j}{\partial x_i}\right)\right] + \frac{\partial p_d}{\partial x_i} = -(\rho - \rho_r)gn_i, \quad i = 1, \ldots, N. \tag{15}$$

Remark 5

Two special cases of the L-model are the variable density model (V-model) and the Boussinesq model (B-model).

Variable density model (V-model)

In some cases, p_T may be considered constant, e.g. (a) when the flow is open to the atmosphere or (b) when one is interested in the steady state only. Then the equation of state (13) reduces to

$$\rho = \frac{p_T}{RT} \equiv \frac{C}{T} \equiv \rho(T), \tag{16}$$

where $C = p_T/R$ is a constant.

Let T_r be a representative temperature and $\rho_r = \rho(T_r)$; then we have

$$\rho(T) = \frac{\rho_r}{1 + \beta_r(T - T_r)}, \tag{17}$$

where $\beta_r = 1/T_r$ is called the thermal expansion coefficient.

Note that when $(T - T_r)/T_r < 1$, equation (17) can be expanded into a Taylor series:

$$\rho(T) = \rho_r\{1 - \beta_r(T - T_r) + [\beta_r(T - T_r)]^2 - \ldots\}. \tag{18}$$

In the heat equation (12) we now have $\mathrm{d}p_T/\mathrm{d}t = 0$ and the L-model reduces to the following V-model.

Continuity equation

$$\frac{\mathrm{D}\rho}{\mathrm{D}t} + \rho\nabla\cdot\mathbf{u} = 0. \tag{19}$$

Momentum equation

$$\rho\frac{\mathrm{D}u_i}{\mathrm{D}t} - \sum_{j=1}^{N}\frac{\partial}{\partial x_j}\left[\mu\left(\frac{\partial u_i}{\partial x_j} + \frac{\partial u_j}{\partial x_i}\right)\right] + \frac{\partial p_d}{\partial x_i} = -(\rho - \rho_r)gn_i, \quad i = 1, \ldots, N. \tag{20}$$

Heat equation

$$\rho C_p\frac{\mathrm{D}T}{\mathrm{D}t} - \sum_{j=1}^{N}\frac{\partial}{\partial x_j}\left(k\frac{\partial T}{\partial x_j}\right) = Q. \tag{21}$$

Equation of state

$$\rho = \rho(T) = \frac{\rho_r}{1 + \beta_r(T - T_r)}. \tag{22}$$

Boussinesq model (B-model)

If the relative change in temperature is small, i.e.

$$\frac{\Delta T}{T} \ll 1, \tag{23}$$

then the density ρ can be considered as constant, i.e. $\rho = \rho_r$. If we also take a first-order approximation to the buoyancy force in the momentum equation (20), then we obtain the Boussinesq model (B-model).

Continuity equation

$$\nabla \cdot \mathbf{u} = 0. \tag{24}$$

Momentum equation

$$\rho \frac{Du_i}{Dt} - \sum_{j=1}^{N} \frac{\partial}{\partial x_j}\left[\mu\left(\frac{\partial u_i}{\partial x_j} + \frac{\partial u_j}{\partial x_i}\right)\right] + \frac{\partial p_d}{\partial x_i} = \rho\beta_r(T - T_r)gn_i, \quad i = 1, \ldots, N. \tag{25}$$

Heat equation

$$\rho C_p \frac{DT}{Dt} - \sum_{j=1}^{N} \frac{\partial}{\partial x_j}\left(k\frac{\partial T}{\partial x_j}\right) = Q. \tag{26}$$

Equation of state

$$\rho = \rho_r = \text{const}. \tag{27}$$

Note. In the conventional strict Boussinesq model the conductivity k and viscosity μ are also considered to be constants.[13,14] However, in the extended Boussinesq model the conductivity k and viscosity μ are allowed to vary with temperature, which leads to an enlarged range of validity when the fluid viscosity exhibits a relatively strong temperature dependence, e.g. for liquids.[13,14]

4. NON-DIMENSIONALIZATION

Define the Rayleigh number $Ra = \beta_r \delta T \rho_r g L^3/\mu_r \alpha_r$. Choosing $U = (\alpha_r/L)\sqrt{(RaPr)}$ and $p_{d,r} = \mu_r U/L$, we have used the following scaling for the non-dimensionalization (quantities with a 'hat' are non-dimensional):

$$x_i = L\hat{x}_i, \qquad \mathbf{u} = U\hat{\mathbf{u}}, \qquad t = \frac{L}{U}\hat{t}, \qquad p_d = p_{d,r}\hat{p}_d, \qquad \rho = \rho_r\hat{\rho},$$

$$T = T_r + \delta T \cdot \hat{T}, \qquad p_T = p_{T,r}\hat{p}_T, \qquad \mu = \mu_r\hat{\mu}, \qquad k = k_r\hat{k}, \qquad Q = \frac{k_r\delta T}{L^2}\hat{Q}.$$

The non-dimensionalized model equations are stated below (with the 'hat' being dropped).

L-model

$$\frac{\mathrm{D}\rho}{\mathrm{D}t} + \rho \nabla \cdot \mathbf{u} = 0, \tag{28}$$

$$\sqrt{\left(\frac{Ra}{Pr}\right)}\rho \frac{\mathrm{D}u_i}{\mathrm{D}t} - \sum_{j=1}^{N} \frac{\partial}{\partial x_j}\left[\mu\left(\frac{\partial u_i}{\partial x_j} + \frac{\partial u_j}{\partial x_i}\right)\right] + \frac{\partial p_{\mathrm{d}}}{\partial x_i} = -\frac{\sqrt{(Ra/Pr)}}{\beta_{\mathrm{r}}\delta T}(\rho - 1)n_i, \quad i = 1, \ldots, N, \tag{29}$$

$$\sqrt{(RaPr)}\rho \frac{\mathrm{D}T}{\mathrm{D}t} - \sum_{j=1}^{N} \frac{\partial}{\partial x_j}\left(k \frac{\partial T}{\partial x_j}\right) = \frac{\sqrt{(RaPr)}}{\beta_{\mathrm{r}}\delta T}\frac{\gamma - 1}{\gamma}\frac{\mathrm{d}p_{\mathrm{T}}}{\mathrm{d}t} + Q, \tag{30}$$

$$\rho = \frac{p_{\mathrm{T}}}{1 + \beta_{\mathrm{r}}\delta T \cdot T}, \tag{31}$$

$$meas(\Omega)\frac{\mathrm{d}p_{\mathrm{T}}}{\mathrm{d}t} + \left(\int_{\Omega} \nabla \cdot \mathbf{u}\, \mathrm{d}\mathbf{x}\right)p_{\mathrm{T}} = \beta_{\mathrm{r}}\delta T \int_{\Omega} \rho \frac{\mathrm{D}T}{\mathrm{D}t}\, \mathrm{d}\mathbf{x}. \tag{32}$$

V-model

$$\frac{\mathrm{D}\rho}{\mathrm{D}t} + \rho \nabla \cdot \mathbf{u} = 0, \tag{33}$$

$$\sqrt{\left(\frac{Ra}{Pr}\right)}\rho \frac{\mathrm{D}u_i}{\mathrm{D}t} - \sum_{j=1}^{N} \frac{\partial}{\partial x_j}\left[\mu\left(\frac{\partial u_i}{\partial x_j} + \frac{\partial u_j}{\partial x_i}\right)\right] + \frac{\partial p_{\mathrm{d}}}{\partial x_i} = -\frac{\sqrt{(Ra/Pr)}}{\beta_{\mathrm{r}}\delta T}(\rho - 1)n_i, \quad i = 1, \ldots, N, \tag{34}$$

$$\sqrt{(RaPr)}\rho \frac{\mathrm{D}T}{\mathrm{D}t} - \sum_{j=1}^{N} \frac{\partial}{\partial x_j}\left(k \frac{\partial T}{\partial x_j}\right) = Q, \tag{35}$$

$$\rho = \frac{1}{1 + \beta_{\mathrm{r}}\delta T \cdot T}. \tag{36}$$

B-model

$$\nabla \cdot \mathbf{u} = 0, \tag{37}$$

$$\sqrt{\left(\frac{Ra}{Pr}\right)}\frac{\mathrm{D}u_i}{\mathrm{D}t} - \sum_{j=1}^{N} \frac{\partial}{\partial x_j}\left[\mu\left(\frac{\partial u_i}{\partial x_j} + \frac{\partial u_j}{\partial x_i}\right)\right] + \frac{\partial p_{\mathrm{d}}}{\partial x_i} = \sqrt{\left(\frac{Ra}{Pr}\right)}Tn_i, \quad i = 1, \ldots N, \tag{38}$$

$$\sqrt{(RaPr)}\frac{\mathrm{D}T}{\mathrm{D}t} - \sum_{j=1}^{N} \frac{\partial}{\partial x_j}\left(k \frac{\partial T}{\partial x_j}\right) = Q. \tag{39}$$

Remark 6

$Ra/Pr = Gr$ is the Grashof number. The Sutherland law[5,6] expressed in the above non-dimensionalized variables becomes

$$k = \frac{(1+\beta_r\delta T\cdot T)^{3/2}(1+S_k)}{1+\beta_r\delta T\cdot T+S_k}, \quad S_k = 0{\cdot}648,$$
$$\mu = \frac{(1+\beta_r\delta T\cdot T)^{3/2}(1-S_\mu)}{1+\beta_r\delta T\cdot T+S_\mu}, \quad S_\mu = 0{\cdot}368.$$

5. SOLUTION BY SEGREGATED TIME STEPPING

Define

$$R_{\mathrm{T}} = \frac{\sqrt{(RaPr)}}{\beta_r\delta T}\frac{\gamma-1}{\gamma}, \qquad R_o = \frac{\sqrt{(Ra/Pr)}}{R_{\mathrm{T}}}.$$

Introduce $\rho^* = \sqrt{(Ra/Pr)}\rho$ and $p_{\mathrm{T}}^* = R_{\mathrm{T}}p_{\mathrm{T}}$. Then we may put the non-dimensionalized L/ V/B-models into the following general forms (with the 'asterisk' being dropped).

Navier–Stokes equation

$$\rho\frac{\mathrm{D}u_i}{\mathrm{D}t} - \sum_{j=1}^{N}\frac{\partial}{\partial x_j}\left[\mu\left(\frac{\partial u_i}{\partial x_j}+\frac{\partial u_j}{\partial x_i}\right)\right] + \frac{\partial p_{\mathrm{d}}}{\partial x_i} = f_i, \quad i=1,\ldots,N, \tag{40}$$

$$\nabla\cdot\mathbf{u} = W(Z,\mathbf{u}). \tag{41}$$

Heat equation

$$\rho Pr\frac{\mathrm{D}T}{\mathrm{D}t} - \sum_{j=1}^{N}\frac{\partial}{\partial x_j}\left(k\frac{\partial T}{\partial x_j}\right) = \frac{\mathrm{d}p_{\mathrm{T}}}{\mathrm{d}t} + Q. \tag{42}$$

Equation of state

$$\rho = \rho(p_{\mathrm{T}}, T). \tag{43}$$

ODE for p_{T} (for L-model only)

$$meas(\Omega)\frac{\mathrm{d}p_{\mathrm{T}}}{\mathrm{d}t} + \left(\int_\Omega \nabla\cdot\mathbf{u}\,\mathrm{d}\mathbf{x}\right)p_{\mathrm{T}} = \frac{\gamma-1}{\gamma}Pr\int_\Omega \rho\frac{\mathrm{D}T}{\mathrm{D}t}\,\mathrm{d}\mathbf{x}. \tag{44}$$

Remark 7

(a)

$$\rho(p_{\mathrm{T}}, T) = \begin{cases} \dfrac{R_o p_{\mathrm{T}}}{(1+\beta_r\delta T\cdot T)} & \text{for L-model,} \\ \dfrac{\sqrt{(Ra/Pr)}}{(1+\beta_r\delta T\cdot T)} & \text{for V-model,} \\ \rho = \sqrt{(Ra/Pr)} & \text{for B-model.} \end{cases} \tag{45}$$

(b)

$$Z = \ln \rho \quad \text{and} \quad W(Z, \mathbf{u}) = \begin{cases} -\left[\dfrac{\partial Z}{\partial t} + (\mathbf{u} \cdot \nabla) Z\right] & \text{for L/V-models,} \\ 0 & \text{for B-model.} \end{cases} \tag{46}$$

(c)

$$f_i = \begin{cases} -(1/\beta_r \delta T)[\rho - \sqrt{(Ra/Pr)}] n_i & \text{for L/V-models,} \\ \rho T n_i & \text{for B-model.} \end{cases} \tag{47}$$

(d) For the V/B models the term dp_{T}/dt on the RHS of (42) should be dropped and the ODE (44) is not needed.

Let t^n be the time at the nth step, Δt be the time step size and $f^{n+\eta}$ denote the value at $t = t^n + \eta \Delta t$ of the function $f(t)$. The segregated time-stepping scheme we propose for solving the non-dimensionalized models (40)–(44) for low-Mach-number flows is given below.

From $\{T^n, \mu^n, k^n, p_{\mathrm{T}}^n, \rho^n, Z^n, \mathbf{u}^n, p_{\mathrm{d}}^n\} \rightarrow \{T^{n+1}, \mu^{n+1}, p_{\mathrm{T}}^{n+1}, \rho^{n+1}, Z^{n+1}, \mathbf{u}^{n+1}, p_{\mathrm{d}}^{n+1}\}$ as follows:

1. Solve for T^{n+1} the heat equation

$$\rho^n Pr \frac{\partial T}{\partial t} + \rho^n Pr (\mathbf{u}^* \cdot \nabla) T - \sum_{j=1}^{N} \frac{\partial}{\partial x_j}\left(k^n \frac{\partial T}{\partial x_j}\right) = Q + \frac{p_{\mathrm{T}}^n - p_{\mathrm{T}}^{n-1}}{\Delta t} \tag{48}$$

   by either the fully implicit (backward Euler) scheme or the Crank–Nicolson scheme; $\mathbf{u}^*$ here may be taken as $\mathbf{u}^n$ or the extrapolation $2\mathbf{u}^n - \mathbf{u}^{n-1}$ for the Euler scheme or $(3\mathbf{u}^n - \mathbf{u}^{n-1})/2$ for the Crank–Nicolson scheme.
2. Calculate $\mu^{n+1} = \mu(T^{n+1})$ and $k^{n+1} = k(T^{n+1})$.
3. (For L-model only.) Solve for p_{T}^{n+1} the ODE (44) by either the fully implicit (backward Euler) scheme or the Crank–Nicolson scheme. Let

$$V = meas(\Omega), \qquad F^* = \int_\Omega \nabla \cdot \mathbf{u}^* \mathbf{dx}, \qquad S^* = \frac{\gamma - 1}{\gamma} Pr \int_\Omega \rho^n \left(\frac{T^{n+1} - T^n}{\Delta t} + (\mathbf{u}^* \cdot \nabla) T^*\right) \mathbf{dx}.$$

   T^* denotes T^{n+1} for the Euler scheme and $(T^{n+1} + T^n)/2$ for the Crank–Nicolson scheme; $\mathbf{u}^*$ is defined as above. The *fully implicit* scheme is

$$V \frac{p_T^{n+1} - p_{\mathrm{T}}^n}{\Delta t} + F^* p_{\mathrm{T}}^{n+1} = S^*. \tag{49}$$

   The *Crank–Nicolson* scheme is

$$V \frac{p_{\mathrm{T}}^{n+1} - p_{\mathrm{T}}^n}{\Delta t} + \frac{F^*}{2}(p_{\mathrm{T}}^{n+1} + p_{\mathrm{T}}^n) = S^*. \tag{50}$$

4. Calculate $\rho^{n+1} = \rho(p_{\mathrm{T}}^{n+1}, T^{n+1})$ and $Z^{n+1} = \ln \rho^{n+1}$.
5. Calculate $\rho^{n+1/2} = \frac{1}{2}(\rho^{n+1} + \rho^n)$ and $Z_{n+1/2} = \ln \rho^{n+1/2}$.

6. Solve for $\{\mathbf{u}^{n+1}, p_{\mathrm{d}}^{n+1}\}$ the following Navier–Stokes equation with variable density and viscosity by the operator-splitting method (which is the topic of Section 6):

$$\rho^{n+1/2}\frac{\partial u_i}{\partial t} - \sum_{j=1}^{N}\frac{\partial}{\partial x_j}\left[\mu^{n+1}\left(\frac{\partial u_i}{\partial x_j}+\frac{\partial u_j}{\partial x_i}\right)\right] + \rho^{n+1/2}(\mathbf{u}\cdot\nabla)u_i + \frac{\partial p_{\mathrm{d}}}{\partial x_i} = f_i^{n+1/2}, \quad i = 1,\ldots,N, \tag{51}$$

$$\nabla\cdot\mathbf{u} = W(Z^{n+1/2},\mathbf{u}), \tag{52}$$

where

$$W(Z^{n+1/2},\mathbf{u}) = \begin{cases} -[(Z^{n+1}-Z^{n})/\Delta t + (\mathbf{u}\cdot\nabla)Z^{n+1/2}] & \text{for L/V-models,} \\ 0 & \text{for B-model.} \end{cases} \tag{53}$$

$$f_i^{n+1/2} = \begin{cases} -(1/\beta_{\mathrm{r}}\delta T)[\rho^{n+1/2} - \sqrt{(Ra/Pr)}]n_i & \text{for L/V-models,} \\ \rho[(T^{n+1}+T^{n})/2]n_i & \text{for B-model.} \end{cases} \tag{54}$$

Remark 8

In the case of closed flow the global mass is conserved. However, the discrete solution p_{T}^{n+1} of the above step 3 does not in general preserve exact global mass conservation, although the deviation is small and is consistent with the discretization error of the solutions (see Section 8 for a discussion on this problem). The numerical results in Section 7 also show that the solutions are not sensitive to this small deviation from global mass conservation. Nevertheless, if we want, we can optionally apply a correction to p_{T}^{n+1} to maintain exact global mass conservation. Denote the discrete solution p_{T}^{n+1} of the above step 3 by p_{T}^{*}; then the correction can be done in the following steps.

(i) Calculate the initial mass

$$M^0 = \int_\Omega \rho^0\,\mathrm{d}\mathbf{x} = \sqrt{(Ra/Pr)}\,meas(\Omega).$$

(ii) Compute

$$\rho* = \frac{R_{\mathrm{o}}p_{\mathrm{T}}^{*}}{1+\beta_{\mathrm{r}}\delta T\cdot T^{n+1}} \quad \text{and} \quad M^{*} = \int_\Omega \rho^{*}\,\mathrm{d}\mathbf{x}.$$

(iii) Compute the correction Δ_p by

$$\Delta p = (M^0 - M^{*}) \Big/ \int_\Omega \frac{R_{\mathrm{o}}}{1+\beta_{\mathrm{T}}\delta T\cdot T^{n+1}}\,\mathrm{d}\mathbf{x}.$$

(iv) Reset $p_{\mathrm{T}}^{n+1} = p_{\mathrm{T}}^{*} + \Delta p$.

6. SOLUTION OF NAVIER–STOKES EQUATION WITH VARIABLE DENSITY AND VISCOSITY BY OPERATOR SPLITTING

6.1. Navier–Stokes equation with variable density and viscosity; its variational formulation

The operator-splitting method is an efficient and robust method for solving the Navier–Stokes equations,[8–12] which enables us to decouple the difficulties in solving the Navier–Stokes equations, i.e. continuity constraints, non-linearity, coupling of velocity components, and the resulting subproblems can be solved by specially designed efficient solvers, e.g. a preconditioned conjugate gradient iterative solver. In this section we extend the operator-splitting method to meet the needs of solving the Navier–Stokes equation with variable density and viscosity, which is the major step in the segregated time-marching solution algorithm of Section 5. For the convenience of describing the operator-splitting method, we consider the following general form of Navier–Stokes equation (N–S) with variable density and viscosity (of which (51), (52) is a special case):

$$\rho\frac{\partial u_i}{\partial t}-\sum_{j=1}^{N}\frac{\partial}{\partial x_j}\left[\mu\left(\frac{\partial u_i}{\partial x_j}+\frac{\partial u_j}{\partial x_i}\right)\right]+\rho(\mathbf{u}\cdot\nabla)u_i+\frac{\partial p}{\partial x_i}=f_i,\quad i=1,\ldots,N, \tag{55}$$

$$\nabla\cdot\mathbf{u}=W(\mathbf{u}), \tag{56}$$

where $\rho=\rho(\mathbf{x})$ and $\mu=\mu(\mathbf{x})$ are known functions of $\mathbf{x}$ and $W(\mathbf{u})$ is a known function of $\mathbf{u}$.

Let Ω be the flow domain and Γ its boundary. We will consider two types of boundary conditions (BCs).

(a) BC1 (enclosed flow):

$$\mathbf{u}=\mathbf{g}=\mathbf{0}\quad\text{on }\Gamma.$$

(b) BC2 (open or partly open flow):

$$\mathbf{u}=\mathbf{g}\quad\text{on }\Gamma_0,\qquad \nu\frac{\partial\mathbf{u}}{\partial\mathbf{n}}=p\mathbf{n}+\mathbf{g}_1\quad\text{on }\Gamma_1,$$

where $\Gamma_0\cup\Gamma_1=\Gamma$.

Let $L^2(\Omega)$ be the Hilbert space of square integrable functions defined over Ω, $H^1(\Omega)$ be the Hilbert space of functions with integrable first-order derivatives and $(H^1(\Omega))^N$ be the space of N-dimensional vector functions each of whose components belongs to $H^1(\Omega)$. For each of the different types of boundary conditions above we define different functional spaces as follows.

(a) For BC1:

$$\mathscr{V}_g=\{\mathbf{v}|\mathbf{v}\in(H^1(\Omega))^N,\mathbf{v}=\mathbf{g}\text{ on }\Gamma\},$$
$$\mathscr{V}_0=\{\mathbf{v}|\mathbf{v}\in(H^1(\Omega))^N,\mathbf{v}=\mathbf{0}\text{ on }\Gamma\},$$
$$\mathscr{H}=\left\{q|q\in L^2(\Omega),\int_\Omega q\,d\mathbf{x}=0\right\}.$$

(b) For BC2:

$$\mathscr{V}_g = \{\mathbf{v} | \mathbf{v} \in (H^1(\Omega))^N, \mathbf{v} = \mathbf{g} \text{ on } \Gamma_0\},$$
$$\mathscr{V}_0 = \{\mathbf{v} | \mathbf{v} \in (H^1(\Omega))^N, \mathbf{v} = \mathbf{0} \text{ on } \Gamma_0\},$$
$$\mathscr{H} = L^2(\Omega).$$

Then the equivalent variational problem (VP) of (N–S) with BC2 type of BC can be stated as follows. Find $\mathbf{u} \in \mathscr{V}_g, p \in L^2(\Omega)$ s.t. $\forall \mathbf{v} \in \mathscr{V}_0, \forall q \in L^2(\Omega)$,

$$\int_\Omega \rho \frac{\partial \mathbf{u}}{\partial t} \cdot \mathbf{v}\, d\mathbf{x} + \int_\Omega \mu \nabla \mathbf{u} \cdot \nabla \mathbf{v}\, d\mathbf{x} + \int_\Omega \rho (\mathbf{u} \cdot \nabla)\mathbf{u} \cdot \mathbf{v}\, d\mathbf{x} - \int_\Omega \mathrm{p} \nabla \cdot \mathbf{v}\, d\mathbf{x} - \int_\Omega (\nabla \mu) \cdot (\mathbf{v} \cdot \nabla)\mathbf{u}\, d\mathbf{x}$$

$$= -\int_\Omega W(\mathbf{u})(\nabla \mu) \cdot \mathbf{v}\, d\mathbf{x} + \int_\Omega \mathbf{f} \cdot \mathbf{v}\, d\mathbf{x} + \int_{\Gamma_1} \mathbf{g}_1 \cdot \mathbf{v}\, d\Gamma, \tag{57}$$

$$\int_\Omega \nabla \cdot \mathbf{u} q\, d\mathbf{x} = \int_\Omega W(\mathbf{u}) q\, d\mathbf{x}. \tag{58}$$

Remark 9

The variational formulation for BC1 type of BC is obtained by dropping the line integral term on the RHS of (57).

6.2. Operator-splitting

Let $\theta \in (0, \frac{1}{3})$ and $\alpha, \beta \in (0, 1)$. The operator-splitting (O–S) scheme for (57), (58) divides each time step into the following three fractional steps.

First fractional step

Find $\mathbf{u}^{n+\theta} \in \mathscr{V}_{g^{n+\theta}}, p^{n+\theta} \in L^2(\Omega)$ s.t. $\forall \mathbf{V} \in \mathscr{V}_0, \forall q \in L^2(\Omega)$,

$$\int_\Omega \frac{\mathbf{u}^{n+\theta} - \mathbf{u}^n}{\theta \Delta t} \cdot \mathbf{v}\, d\mathbf{x} + \alpha \int_\Omega \mu \nabla \mathbf{u}^{n+\theta} \cdot \nabla \mathbf{v}\, d\mathbf{x} - \int_\Omega p^{n+\theta} \nabla \cdot \mathbf{v}\, d\mathbf{x}$$
$$= -\beta \int_\Omega \mu \nabla \mathbf{u}^n \cdot \nabla \mathbf{v}\, d\mathbf{x} - \int_\Omega \rho (\mathbf{u}^n \cdot \nabla) \mathbf{u}^n \cdot \mathbf{v}\, d\mathbf{x} + \int_\Omega (\nabla \mu) \cdot (\mathbf{v} \cdot \nabla) \mathbf{u}^n\, d\mathbf{x}$$
$$- \int_\Omega W(\mathbf{u}^n)(\nabla \mu) \cdot \mathbf{v}\, d\mathbf{x} + \int_\Omega \mathbf{f}^{n+\theta} \cdot \mathbf{v}\, d\mathbf{x} + \int_{\Gamma_1} \mathbf{g}_1^{n+\theta} \cdot \mathbf{v}\, d\Gamma, \tag{59}$$

$$\int_\Omega \nabla \cdot \mathbf{u}^{n+\theta} q\, d\mathbf{x} = \int_\Omega W(\mathbf{u}^n) q\, d\mathbf{x}. \tag{60}$$

Second fractional step

Find $\mathbf{u}^{n+1-\theta} \in \mathscr{V}_{g^{n+1-\theta}}$ s.t. $\forall \mathbf{v} \in \mathscr{V}_0$,

$$\int_\Omega \rho \frac{\mathbf{u}^{n+1-\theta} - \mathbf{u}^{n+\theta}}{(1-2\theta)\Delta t} \cdot \mathbf{v}\,\mathrm{d}\mathbf{x} + \beta \int_\Omega \mu \nabla \mathbf{u}^{n+1-\theta} \cdot \nabla \mathbf{v}\,\mathrm{d}\mathbf{x} + \int_\Omega \rho(\mathbf{u}^{n+1-\theta} \cdot \nabla)\mathbf{u}^{n+1-\theta} \cdot \mathbf{v}\,\mathrm{d}\mathbf{x} - \int_\Omega (\nabla\mu) \cdot (\mathbf{v} \cdot \nabla)\mathbf{u}^{n+1-\theta}\,\mathrm{d}\mathbf{x}$$

$$= -\alpha \int_\Omega \mu \nabla \mathbf{u}^{n+\theta} \cdot \nabla \mathbf{v}\,\mathrm{d}\mathbf{x} + \int_\Omega p^{n+\theta} \nabla \cdot \mathbf{v}\,\mathrm{d}\mathbf{x} - \int_\Omega W(\mathbf{u}^n)(\nabla\mu) \cdot \mathbf{v}\,\mathrm{d}\mathbf{x} + \int_\Omega \mathbf{f}^{n+1-\theta}\mathbf{v}\,\mathrm{d}\mathbf{x} + \int_{\Gamma_1} \mathbf{g}_1^{n+1-\theta} \cdot \mathbf{v}\,\mathrm{d}\Gamma. \tag{61}$$

Remark 10

For the linearized O–S scheme the third term on the LHS of (61) should be replaced by

$$\int_\Omega \rho(\mathbf{u}^{n+\theta} \cdot \nabla)\mathbf{u}^{n+1-\theta} \cdot \mathbf{v}\,\mathrm{d}\mathbf{x}. \tag{62}$$

Third fractional step

Find $\mathbf{u}^{n+1} \in \mathscr{V}_{g^{n+1}}, p^{n+1} \in L^2(\Omega)$ s.t. $\forall \mathbf{v} \in \mathscr{V}_0, \forall q \in L^2(\Omega)$,

$$\int_\Omega \rho \frac{\mathbf{u}^{n+1} - \mathbf{u}^{n+1-\theta}}{\theta\Delta t} \cdot \mathbf{v}\,\mathrm{d}\mathbf{x} + \alpha \int_\Omega \mu \nabla \mathbf{u}^{n+1} \cdot \nabla \mathbf{v}\,\mathrm{d}\mathbf{x} - \int_\Omega p^{n+1} \nabla \cdot \mathbf{v}\,\mathrm{d}\mathbf{x}$$
$$= -\beta \int_\Omega \mu \nabla \mathbf{u}^{n+1-\theta} \cdot \nabla \mathbf{v}\,\mathrm{d}\mathbf{x} - \int_\Omega \rho(\mathbf{u}^{n+1-\theta} \cdot \nabla)\mathbf{u}^{n+1-\theta} \cdot \mathbf{v}\,\mathrm{d}\mathbf{x} + \int_\Omega (\nabla\mu) \cdot (\mathbf{v} \cdot \nabla)\mathbf{u}^{n+1-\theta}\,\mathrm{d}\mathbf{x}$$
$$- \int_\Omega W(\mathbf{u}^{n+1-\theta})(\nabla\mu) \cdot \mathbf{v}\,\mathrm{d}\mathbf{x} + \int_\Omega \mathbf{f}^{n+1} \cdot \mathbf{v}\,\mathrm{d}\mathbf{x} + \int_{\Gamma_1} \mathbf{g}_1^{n+1} \cdot \mathbf{v}\,\mathrm{d}\Gamma,$$

$$\int_\Omega \nabla \cdot \mathbf{u}^{n+1} q\,\mathrm{d}\mathbf{x} = \int_\Omega W(\mathbf{u}^{n+1-\theta}) q\,\mathrm{d}\mathbf{x}. \tag{63}$$

The subproblems at the first and third fractional steps are of the type of steady quasi-Stokes problem (QS) with variable density and viscosity. Find $\mathbf{u} \in \mathscr{V}_g, p \in L^2(\Omega)$ s.t. $\forall \mathbf{v} \in \mathscr{V}_0, \forall q \in (\Omega)$,

$$\alpha_0 \int_\Omega \rho \mathbf{u} \cdot \mathbf{v}\,\mathrm{d}\mathbf{x} + \int_\Omega \mu_1 \nabla \mathbf{u} \cdot \nabla \mathbf{v}\,\mathrm{d}\mathbf{x} - \theta \int_\Omega p \nabla \cdot \mathbf{v}\,\mathrm{d}\mathbf{x} = \int_\Omega \mathbf{f} \cdot \mathbf{v}\,\mathrm{d}\mathbf{x}, \tag{64}$$

$$\int_\Omega \nabla \cdot \mathbf{u} q\,\mathrm{d}\mathbf{x} = \int_\Omega W q\,\mathrm{d}\mathbf{x}, \tag{65}$$

with $\alpha_0 = 1/\Delta t$ and $\mu_1 = \alpha\theta\mu$.

The subproblem at the second fractional step is of the type of (non-linear) diffusion-convection problem (DC). Find $\mathbf{u} \in \mathscr{V}_g$ s.t. $\forall \mathbf{v} \in \mathscr{V}_0$,

$$\alpha_0 \int_\Omega \rho \mathbf{u} \cdot \mathbf{v}\,\mathrm{d}\mathbf{x} + \int_\Omega \mu_2 \nabla \mathbf{u} \cdot \nabla \mathbf{v}\,\mathrm{d}\mathbf{x} + b_n \int_\Omega \rho(\mathbf{u} \cdot \nabla)\mathbf{u} \cdot \mathbf{v}\,\mathrm{d}\mathbf{x} - b_n \int_\Omega (\nabla\mu) \cdot (\mathbf{v} \cdot \nabla)\mathbf{u}\,\mathrm{d}\mathbf{x} = \int_\Omega \mathbf{f} \cdot \mathbf{v}\,\mathrm{d}\mathbf{x}, \tag{66}$$

with $b_n = 1 - 2\theta$ and $\mu_2 = \beta b_n \mu$.

A good choice of θ is $1 - 1/\sqrt{2}$; α and β can be chosen s.t. $\mu_1 = \mu_2$ so that both subproblems have the same part of the Helmholtz operator, which will give the same matrices in discretizations.

The subproblems (QS) can be solved by a preconditioned conjugate gradient (CG) method. The subproblem (DC) can be reformulated as a least squares problem and solved by a preconditioned conjugate gradient method.

6.3. *CG scheme for QS*

The steady state quasi-Stokes problem (64), (65) is a special case of the following general *steady quasi-Stokes* problem (QS) with variable density and viscosity. Find $\mathbf{u} \in \mathscr{V}_g$, $p \in L^2(\Omega)$ s.t. $\forall \mathbf{v} \in \mathscr{V}_0, \forall q \in L^2(\Omega)$,

$$\alpha \int_\Omega \rho \mathbf{u} \cdot \mathbf{v} \, d\mathbf{x} + \int_\Omega \nu \nabla \mathbf{u} \cdot \nabla \mathbf{v} \, d\mathbf{x} - \int_\Omega p \nabla \cdot \mathbf{v} \, d\mathbf{x} = \int_\Omega \mathbf{f} \cdot \mathbf{v} \, d\mathbf{x}, \tag{67}$$

$$\int_\Omega \nabla \cdot \mathbf{u} q \, d\mathbf{x} = \int_\Omega W q \, d\mathbf{x}, \tag{68}$$

where α is a constant, ρ, ν and W are known functions of the space co-ordinates $\mathbf{x}$ and $\mathbf{f}$ is a known vector function of $\mathbf{x}$. This problem (QS) can be solved by the following preconditioned conjugate gradient iteration scheme.

Step 0. Initialization

(1) $p^0 \in L^2(\Omega)$ given.
(2) Solve for $\mathbf{u}^0 \in \mathscr{V}_g$ s.t. $\forall \mathbf{v} \in \mathscr{V}_0$,

$$\alpha \int_\Omega \rho \mathbf{u}^0 \cdot \mathbf{v} \, d\mathbf{x} + \int_\Omega \nu \nabla \mathbf{u}^0 \cdot \nabla \mathbf{v} \, d\mathbf{x} = \int_\Omega p^0 \nabla \cdot \mathbf{v} \, d\mathbf{x} + \int_\Omega \mathbf{f} \cdot \mathbf{v} \, d\mathbf{x}.$$

(3) Solve for $Q^0 \in \mathscr{H}$ s.t. $\forall q \in L^2(\Omega)$,

$$\int_\Omega Q^0 q \, d\mathbf{x} = \int_\Omega (\nabla \cdot \mathbf{u}^0 - W) q \, d\mathbf{x}.$$

(4) Solve for Φ^0 the Poisson equation

$$-\Delta \Phi^0 = Q^0,$$

with BCs $\partial \Phi^0 / \partial n = 0$ on Γ_0 and $\Phi^0 = 0$ on Γ_1.

Remark 11

For BC1 type of boundary condition the BC here should be replaced by $\partial \Phi^0 / \partial n = 0$ on Γ, plus the condition $\int_\Omega \Phi^0 \, d\mathbf{x} = 0$.

(5) Set $g^0 = mean(\nu) Q^0 + \alpha \, mean(\rho) \Phi^0$, where $mean(\cdot) = \int_\Omega \cdot \, d\mathbf{x} / meas(\Omega)$.
(6) Set $w^0 = g_0$.

Then for $n \geqslant 0$, with p^n, $\mathbf{u}^n$, g^n and w^n known, obtain p^{n+1}, $\mathbf{u}^{n+1}$, g^{n+1} and w^{n+1} as follows.

Step 1. Descent

(7) Solve for $\boldsymbol{\chi}^n \in \mathscr{V}_0$ s.t. $\forall \mathbf{v} \in \mathscr{V}_0$,

$$\alpha \int_\Omega \rho \boldsymbol{\chi}^n \cdot \mathbf{v}\, d\mathbf{x} + \int_\Omega \nu \nabla \boldsymbol{\chi}^n \cdot \nabla \mathbf{v}\, d\mathbf{x} = \int_\Omega w^n \nabla \cdot \mathbf{v}\, d\mathbf{x}.$$

(8) Compute

$$\rho_n = \frac{\int_\Omega (\nabla \cdot \mathbf{u}^n - W) w^n\, d\mathbf{x}}{\int_\Omega \nabla \cdot \boldsymbol{\chi}^n w^n\, d\mathbf{x}} = \frac{\int_\Omega Q^n w^n\, d\mathbf{x}}{\int_\Omega \nabla \cdot \boldsymbol{\chi}^n w^n\, d\mathbf{x}}.$$

(9) Set $p^{n+1} = p^n - \rho_n w^n$ and $\mathbf{u}^{n+1} = \mathbf{u}^n - \rho_n \boldsymbol{\chi}^n$.

(10) Solve for $Q^{n+1} \in \mathscr{H}$ s.t. $\forall q \in L^2(\Omega)$,

$$\int_\Omega Q^{n+1} q\, d\mathbf{x} = \int_\Omega (\nabla \cdot \mathbf{u}^{n+1} - W) q\, d\mathbf{x}.$$

(11) Solve for Φ^{n+1} the Poisson equation

$$-\Delta \Phi^{n+1} = Q^{n+1},$$

with BCs $\partial \Phi^{n+1}/\partial n = 0$ on Γ_0 and $\Phi^{n+1} = 0$ on Γ_1.

Remark 12

For BC1 type of boundary condition the BC here should be replaced by $\partial \Phi^{n+1}/\partial n = 0$ on Γ, plus the condition $\int_\Omega \Phi^{n+1}\, d\mathbf{x} = 0$.

(12) Set $g^{n+1} = mean(\nu) Q^{n+1} + \alpha\, mean(\rho) \Phi^{n+1}$.

(13) Test convergence: if $\int_\Omega Q^{n+1} g^{n+1}\, d\mathbf{x} \leqslant \delta$, take $p = p^{n+1}$ and $\mathbf{u} = \mathbf{u}^{n+1}$ and stop iteration; otherwise go to (14).

Step 2. Construct new descent direction

(14) Compute

$$\gamma_n = \frac{\int_\Omega Q^{n+1} g^{n+1}\, d\mathbf{x}}{\int_\Omega Q^n g^n\, d\mathbf{x}}.$$

(15) Set $w^{n+1} = g^{n+1} + \gamma_n w^n$.

(16) Do $n := n + 1$, go to (7) and repeat the process.

6.4. CG scheme for NL

The diffusion–convection (66) is a special case of the following general non-linear diffusion–convection problem (DC) with variable density and viscosity. Find $\mathbf{u} \in \mathscr{V}_g$ s.t. $\forall \mathbf{v} \in \mathscr{V}_0$,

$$\alpha \int_\Omega \rho \mathbf{u} \cdot \mathbf{v}\, d\mathbf{x} + \int_\Omega \nu \nabla \mathbf{u} \cdot \nabla \mathbf{v}\, d\mathbf{x} + b_n \int_\Omega \rho (\mathbf{u} \cdot \nabla) \mathbf{u} \cdot \mathbf{v}\, d\mathbf{x} - b_n \int_\Omega (\nabla \nu_o) \cdot (\mathbf{v} \cdot \nabla) \mathbf{u}\, d\mathbf{x} = \int_\Omega \mathbf{f} \cdot \mathbf{v}\, d\mathbf{x}, \tag{69}$$

where α and b_n are constants, ρ, ν and ν_0 are known functions of the space co-ordinates $\mathbf{x}$ and $\mathbf{f}$ is a known vector function of $\mathbf{x}$.

Remark 13

For the linearized O–S scheme the third term on the LHS of (69) should be replaced by

$$b_n \int_\Omega \rho(\mathbf{z}\cdot\nabla)\mathbf{u}\cdot\mathbf{v}\,d\mathbf{x},$$

where $\mathbf{z}$ is a known vector function of $\mathbf{x}$. In the following discussions the corresponding changes will also be needed.

Define the scalar product in $\mathcal{V}_g$ (and $\mathcal{V}_0$) as

$$((\mathbf{v},\mathbf{w})) = \alpha \int_\Omega \rho\mathbf{v}\cdot\mathbf{w}\,d\mathbf{x} + \int_\Omega \nu\nabla\mathbf{v}\cdot\nabla\mathbf{w}\,d\mathbf{x}. \tag{70}$$

Define $\mathbf{y} \equiv \mathbf{y}(\mathbf{u}) \in \mathcal{V}_0$ s.t.

$$\alpha \int_\Omega \rho\mathbf{y}\cdot\mathbf{v}\,d\mathbf{x} + \int_\Omega \nu\nabla\mathbf{y}\cdot\nabla\mathbf{v}\,d\mathbf{x}$$

$$= \alpha \int_\Omega \rho\mathbf{u}\cdot\mathbf{v}\,d\mathbf{x} + \int_\Omega \nu\nabla\mathbf{u}\cdot\nabla\mathbf{v}\,d\mathbf{x} + b_n \int_\Omega \rho(\mathbf{u}\cdot\nabla)\mathbf{u}\cdot\mathbf{v}\,d\mathbf{x} - b_n \int_\Omega (\nabla\nu_0)\cdot(\mathbf{v}\cdot\nabla)\mathbf{u}\,d\mathbf{x} - \int_\Omega \mathbf{f}\cdot\mathbf{v}\,d\mathbf{x}. \tag{71}$$

Define on $\mathcal{V}_g$ the functional

$$\mathcal{J}(\mathbf{v}) = \tfrac{1}{2}((\mathbf{y},\mathbf{y})). \tag{72}$$

Then (DC) is equivalent to the following least squares problem (LS):

$$\text{find } \mathbf{u} \in \mathcal{V}_g \quad \text{s.t.} \quad \mathcal{J}(\mathbf{u}) \leqslant \mathcal{J}(\mathbf{v}) \quad \forall \mathbf{v} \in \mathcal{V}_g. \tag{73}$$

This least squares problem (LS) can be solved by the following preconditioned conjugate gradient iteration scheme

Step 0. Initialization

(1) $\mathbf{u}^0 \in \mathcal{V}_g$ given.
(2) Solve for $\mathbf{g}^0 \in \mathcal{V}_0$ s.t. $\forall \mathbf{v} \in \mathcal{V}_0$,

$$\alpha \int_\Omega \rho\mathbf{g}^0\cdot\mathbf{v} + \int_\Omega \nu\nabla\mathbf{g}^0\cdot\nabla\mathbf{v}\,d\mathbf{x} = \langle \mathcal{J}'(\mathbf{u}^0), \mathbf{v}\rangle.$$

(3) Set $\mathbf{w}^0 = \mathbf{g}^0$.

Then for $n \geqslant 0$, with u^n, g^n, w^n known, obtain $u^{n+1}, g^{n+1}, w^{n+1}$ as follows:

Step 1. Descent

(4) Find $\eta_n \in \mathbb{R}$ s.t. $\mathcal{J}(\mathbf{u}^n - \eta_n\mathbf{w}^n) \leqslant \mathcal{J}(\mathbf{u}^n - \eta\mathbf{w}^n), \forall \eta \in \mathbb{R}$, where $\mathbb{R}$ is the space of all real numbers.
(5) Set $\mathbf{u}^{n+1} = \mathbf{u}^n - \eta_n\mathbf{w}^n$.

(6) Solve for $\mathbf{g}^{n+1} \in \mathscr{V}_0$ s.t. $\forall \mathbf{v} \in \mathscr{V}_0$,

$$\alpha \int_\Omega \rho \mathbf{g}^{n+1} \cdot \mathbf{v} + \int_\Omega \nu \nabla \mathbf{g}^{n+1} \cdot \nabla \mathbf{v} \, d\mathbf{x} = \langle \mathscr{J}'(\mathbf{u}^{n+1}), \mathbf{v} \rangle.$$

(7) Test convergence: if $\mathscr{J}(\mathbf{u}^{n+1}) \leqslant \delta$, take $\mathbf{u} = \mathbf{u}^{n+1}$ and stop iteration; otherwise go to (8).

Step 2. Construct new descent direction

(8) Compute

$$\gamma_n = \frac{((\mathbf{g}^{n+1}, \mathbf{g}^{n+1}))}{((\mathbf{g}^n, \mathbf{g}^n))}.$$

(9) Set $\mathbf{w}^{n+1} = \mathbf{g}^{n+1} + \gamma_n \mathbf{w}^n$.
(10) Do $n := n + 1$, go to (4) and repeat the process.

Remark 14

A simple perturbation analysis shows that

$$\begin{aligned} \langle \mathscr{J}'(\mathbf{u}), \mathbf{v} \rangle = \alpha \int_\Omega \rho \mathbf{y} \cdot \mathbf{v} \, d\mathbf{x} + \int_\Omega \nu \nabla \mathbf{y} \cdot \nabla \mathbf{v} \, d\mathbf{x} + b_n \int_\Omega \rho (\mathbf{u} \cdot \nabla) \mathbf{v} \cdot \mathbf{y} \, d\mathbf{x} \\ + b_n \int_\Omega \rho (\mathbf{v} \cdot \nabla) \mathbf{u} \cdot \mathbf{y} \, d\mathbf{x} - b_n \int_\Omega (\nabla \nu_o) \cdot (\mathbf{y} \cdot \nabla) \mathbf{v} \, d\mathbf{x}. \end{aligned} \tag{74}$$

Remark 15

Let $\mathbf{y}_\eta^n = \mathbf{y}(\mathbf{u}^n - \eta \mathbf{w}^n)$; then we have

$$\mathbf{y}_\eta^n = \mathbf{y}^n - \eta \mathbf{y}_1^n + \eta^2 \mathbf{y}_2^n,$$

with
(a) $\mathbf{y}^n = \mathbf{y}(\mathbf{u}^n)$,
(b) $\mathbf{y}_1^n \in \mathscr{V}_0$ s.t. $\forall \mathbf{v} \in \mathscr{V}_0$,

$$\alpha \int_\Omega \rho \mathbf{y}_1^n \cdot \mathbf{v} \, d\mathbf{x} + \int_\Omega \nu \nabla \mathbf{y}_1^n \cdot \nabla \mathbf{v} \, d\mathbf{x} = \alpha \int_\Omega \rho \mathbf{w}^n \cdot \mathbf{v} \, d\mathbf{x} + \int_\Omega \nu \nabla \mathbf{w}^n \cdot \nabla \mathbf{v} \, d\mathbf{x}$$

$$+ b_n \int_\Omega \rho (\mathbf{u}^n \cdot \nabla) \mathbf{w}^n \cdot \mathbf{v} \, d\mathbf{x} + b_n \int_\Omega \rho (\mathbf{w}^n \cdot \nabla) \mathbf{u}^n \cdot \mathbf{v} \, d\mathbf{x} - b_n \int_\Omega (\nabla \nu_o) \cdot (\mathbf{v} \cdot \nabla) \mathbf{w}^n \, d\mathbf{x}, \tag{75}$$

(c) $\mathbf{y}_2^n \in \mathscr{V}_0$ s.t. $\forall \mathbf{v} \in \mathscr{V}_0$,

$$\alpha \int_\Omega \rho \mathbf{y}_2^n \cdot \mathbf{v} \, d\mathbf{x} + \int_\Omega \nu \nabla \mathbf{y}_2^n \cdot \nabla \mathbf{v} \, d\mathbf{x} = b_n \int_\Omega \rho (\mathbf{w}^n \cdot \nabla) \mathbf{w}^n \cdot \mathbf{v} \, d\mathbf{x}. \tag{76}$$

The function $\mathscr{J}(\mathbf{u}^n - \eta \mathbf{w}^n)$ is a *quartic polynomial* of η. Therefore its minimization reduces mainly to finding the root of a cubic polynomial by Newton's method.

7. NUMERICAL RESULTS

8.1. Comparison with exact limiting solution

Consider the natural convectin of a perfect gas in a vertical slot of width L and height H with left and right wall temperatures T_h and T_c respectively, where $T_h > T_c$. Let $T_r = (T_h + T_c)/2$, $\delta T = T_h - T_c$ and the Rayleigh number Ra be as defined in Section 4. Chenoweth and Paolucci[6] derived the exact velocity and temperature profiles of a fully developed one-dimensional flow which exists in the mid-region of the vertical slot when $Ra < Ra_c$ and the aspect ratio $A = H/L > A_d$. For the Prandtl number $Pr = 0{\cdot}71$ and $0 \leqslant \varepsilon = \delta T/2T_r \leqslant 0{\cdot}6$ they stated that

$$Ra_c \approx 8 \times 10^3 Pr(1 - \varepsilon^3), \qquad A_d \approx (2 + Ra/400)/(1 - \varepsilon^3).$$

In order to verify our solution algorithm, we have compared our numerical results with the exact solution data for the two test cases below. Note that all the quantities appearing in the figures and tables of this sectin are non-dimensional with the scaling given in Section 4, except that quantities in Tables I and II are in the same scaling as used in the figures of Chenoweth and paolucci.[6] Note also that the exact solution data in Tables I and II are obtained by measurements from the figures of Chenoweth and Paolucci.[6] In the non-dimensional co-ordinates (x, y) the flow domain is a rectangle $[0, 1] \times [0, A]$. In Tables I and II the critical point x-co-ordinates X_1, X_0, X and X_n on the mid-section $y = A/2$ are defined as follows: X_1—where $T = 0$; X_0—where velocity y-component $u_y = 0$; X_p—where $u_y = u_{y,\max}$; X_n—where $u_y = u_{y,\min}$.

Test Problem 1

As the first test case, we choose $\varepsilon = 0{\cdot}6, A = 10, Ra = 10^3, Pr = 0{\cdot}71$ and $T_r = 300$ K and consider a closed slot, i.e. with both ends closed. Both solutions of the L-model with correction to p_T^{n+1} for mass conservation (denoted by A-sln.) and without correction (denoted by B-sln.) are shown in Table I and Figures 1 and 2. A graded mesh of 720 rectangular elements with 2305 nodes (see Figure 14(a)) is used for this problem. Without correction to p_T^{n+1} the resultant deviation from mass conservation is less than 0·8%. Table I and Figures 1 and 2 show that the solution is not sensitive to this small deviation. The difference between the two solutions is less than 0·8%. Compared with the exact solution, both solutions are quite accurate, with errors less than 2%, which is smaller than the difference of 3% between the exact solution and the numerical Navier–Stokes solution reported by Chenoweth and Paolucci.[6] Note that the relatively larger error of 1·4% in X_n is due to the linear interpolation used in the velocity profile (Figure 1). A quadratic interpolation will give $X_n = 0{\cdot}8792$, with a smaller error of 0·7%.

Table I. A-sln.—with correction to p_T^{n+1}; B-sln.—without correction

	Exact sln.	A-sln.	B-sln.	Error in B	Diff. of A, B
X_1	0·6360	0·6374	0·6374	0·2%	0·0%
X_0	0·6360	0·6374	0·6374	0·2%	0·0%
X_p	0·2900	0·2894	0·2894	0·2%	0·0%
X_n	0·8730	0·8851	0·8851	1·4%	0·0%
$u_{y,\max}$	0·0922	0·0981	0·0974	1·8%	0·7%
$u_{y,\min}$	−0·0938	−0·0927	−0·0920	1·9%	0·8%

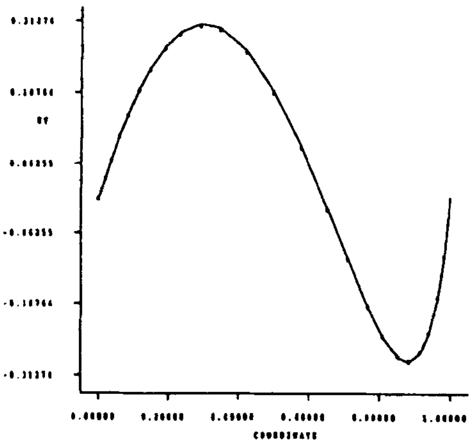

Figure 1. Velocity profile along $y = 5$: full curve, with correction to p_T^{n+1}; points, without correction

Test Problem 2

As the second test case, we consider an open slot, i.e. with both ends open, and choose $\varepsilon = 0{\cdot}6, A = 10, Ra = 10^3, Pr = 0{\cdot}71$ and $T_r = 300$ K, the same as in the first case. In this case we no longer have global mass conservation. The exact solution of Chenoweth and Paolucci[6] for this open slot is valid under the assumption $p_T = 1$; thus the V-model should be used. The same mesh as for the first case has been used for its solution. Table II compares the V-model solution with the exact solution and shows very good accuracy, with errors substantially smaller than the difference of 3% between the exact solution and the numerical Navier–Stokes solution reported by Chenoweth and Paolucci.[6] Note also that the relatively larger error of 1·4% in X_n is again due to the linear interpolation used in the velocity profile (Figure 3).

Figures 3 and 4 show the velocity and temperature profiles along the mid-section $y = 5$. Note that the profiles shown by Figures 1–4 are very close to those of Chenoweth and Paolucci.[6] The above comparision of our results with the exact solutions for the two test cases clearly validates our solution algorithm for the L/V-models. In particular, our algorithm, unlike some other algorithms, e.g. that of

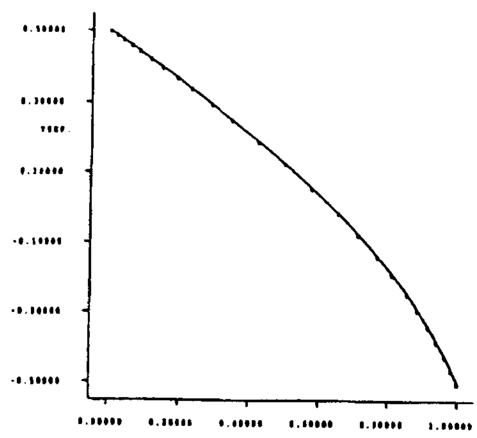

Figure 2. Temperature profile along $y = 5$: full curve, correction to p_T^{n+1}; points, without correction

Table II. V-sln.—solution of V-model

	Exact sln.	V-sln	Error in V-sln.
X_1	0·63600	0·63740	0·2%
X_0	0·63600	0·63740	0·2%
X_p	0·29000	0·28940	0·2%
X_n	0·87300	0·88510	1.4%
$u_{y,\max}$	0·09846	0·09845	0·01%
$u_{y,\min}$	−0·09615	−0·09618	0·03%

Chenoweth and Paolucci,[5] does not rely on the correction to p_{T}^{n+1} for global mass conservation to maintain solution accuracy, so it can be applied to more general cases where such a correction is either impossible or unfeasible. Especially in the case where global mass conservation no longer holds, algorithms depending on such a correction to maintain solution accuracy cannot be used safely, but our algorithm can still be directly applied with confidence.

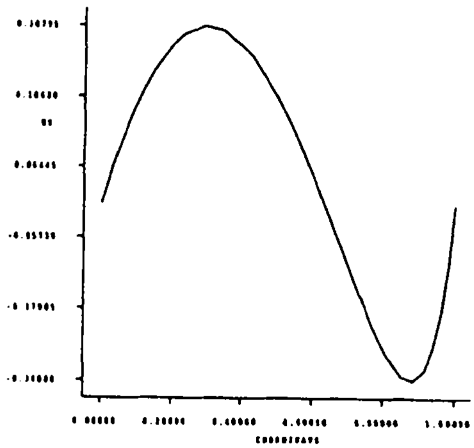

Figure 3. Velocity profile along $y=5$

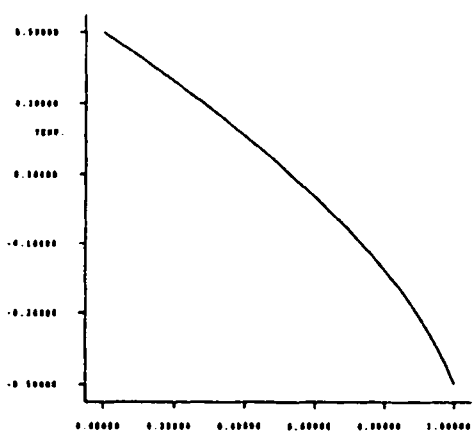

Figure 4. Temperature profile along $y=5$

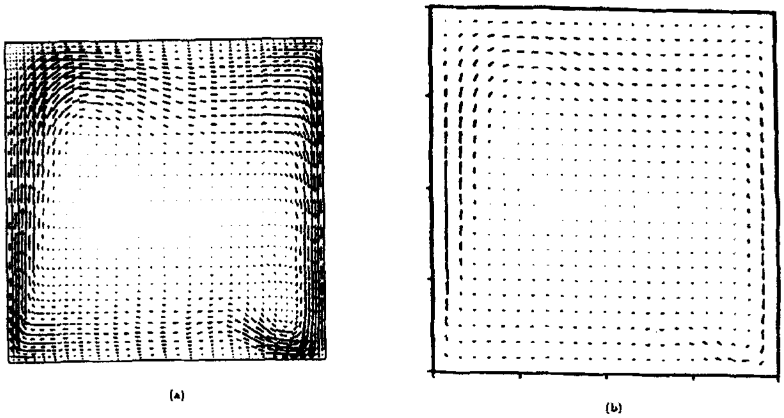

Figure 5. Velocity fields: (a) L-model; (b) Chenoweth and Paolucci[5]

7.2. Comparison with known numerical results

Test Problem 3

We consider a closed square ($A = 1$) with $\varepsilon = 0{\cdot}6, Ra = 10^6, Pr = 0{\cdot}71$ and $T_r = 300$ K and compare our L-model solution with that of Chenoweth and Paolucci.[5] Figures 5(a) and 5(b) show the velocity fields by our L-model solution and Chenoweth and Paolucci's respectively. Figures 6(a) and 6(b) show corresponding isotherm fields. Figure 7 shows the streamline plot of our L-model solution. Figure 8 shows the graded mesh of 576 rectangular elements with 1825 nodes used for this problem.

Figures 5 and 6 show that our solution is very close to that of Chenoweth and Paolucci. Both solutions have very similar asymmetry. There is a very pronounced shift of the primary vortex both towards the cold wall and downwards towards the lower end of the cavity. From Figures 5 and 7 we also see the appearance of two weak secondary vortices inside the primary roll as observed by Chenoweth and Paolucci.[5] The reason for the appearance of this asymmetry and the secondary vortices has been explained by Chenoweth and Paolucci.[5]

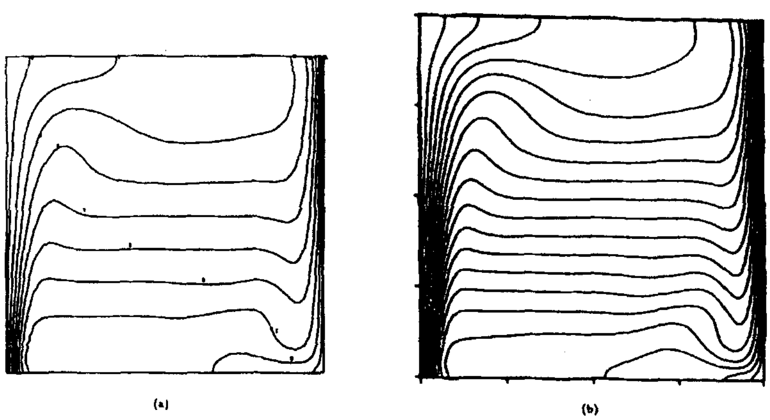

Figure 6. Isotherm fields: (a) L-models; (b) Chenoweth and Paolucci[5]

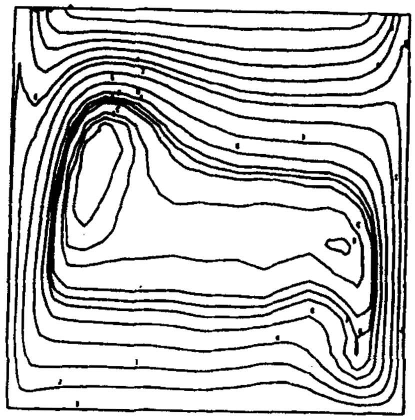

Figure 7. Stream lines of L-model solution

Test Problem 4

To validate the B-model solution (i.e. the Boussinesq case), we consider the same geometry as for the third test problem, with $Pr = 0{\cdot}71$. Our B-model solutions are compared with FIDAP's (FIDAP is a well-known commercial finite element CFD package which has a steady state Boussinesq solver using a fully coupled method). The same mesh as in Figure 8 is used both for our B-model solution and for FIDAP's.

Figures 9(a) and 9(b) show the streamlines by our B-model solution and FIDAP's respectively for the case of $Ra = 10^6$ and $T_r = 300$ K. Note that both solutions predict the same maximum streamfunction value of 0·01990. Figures 10(a) and 10(b) show the corresponding isotherm fields.

Note that a benchmark solution by de Vahl Davis[7] based upon the Boussinesq model for $Ra = 10^6$ and $Pr = 0{\cdot}71$ has an average Nusselt number of 8·798 along the hot wall. Our B-model solution has an average Nusselt number of 8·824, which is a very good prediction, with an error less than 0·3%. The FIDAP solution has an average Nusselt number of 8·893, which, with an error of 1·1%, is slightly less accurate than our B-model solution.

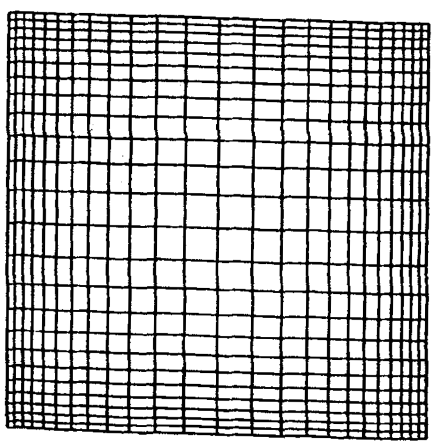

Figure 8. Mesh for $Ra = 10^6$ and $A = 1$

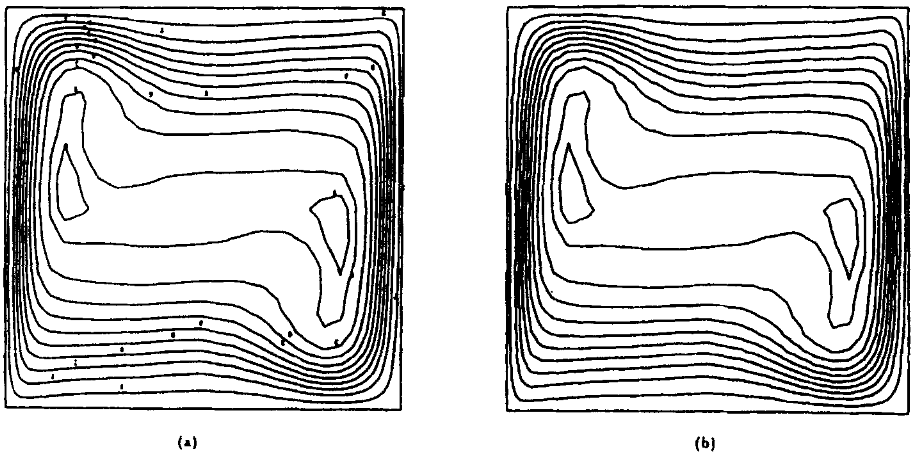

Figure 9. Streamlines for $Ra = 10^6$: (a) B-model; (b) FIDAP

Listed in Table II are the average Nusselt numbers along the hot wall for three different cases predicted by FIDAP, our B-model and our L-model. Note that $T_r = 325$ K is used for all three cases.

Figures 9 and 10 and Table III show clearly that our B-model solutions are almost identical with FIDAP's solutions. Our B-model solution is clearly validated by the above comparison results. Table III also indicates that the B-model solution is close to the L-model solution when the relative change in temperature $\delta T/T_r = 2\varepsilon$ is below about 25%. This is consistent with the statement by Gray and Giorgini[13] that the Boussinesq model is a valid approximation to low-Mach-number air flows if the relative change in temperature $\delta T/T_r = 2\varepsilon \leqslant 0{\cdot}1$.

Table III. Average Nusselt number along hot wall: Nu_F, FIDAP; Nu_B, B-model; Nu_L, L-model

Ra	ε	Nu_F	Nu_B	Nu_L	Diff. of Nu_F, Nu_B	Diff. of Nu_B, Nu_L
10^4	0·013	2·245	2·245	2·237	0·00%	0·36%
10^5	0·130	4·527	4·522	4·358	0·11%	3·76%
10^6	1·300	8·893	8·824	6·795	0·78%	29·86%

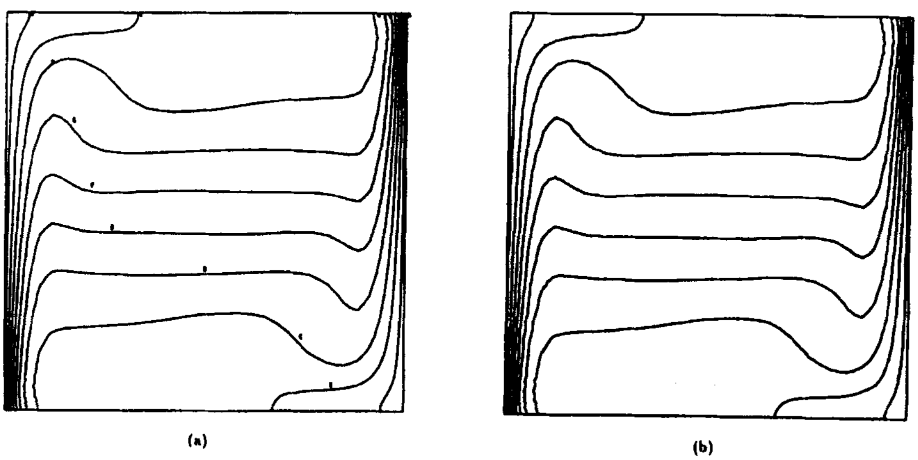

Figure 10. Isotherm fields for $Ra = 10^6$: (a) B-model; (b) FIDAP

According to our numerical tests, taking a constant starting value, FIDAP fails to reach a solution for $Ra = 10^6$ owing to divergence of the iterations. This indicated that FIDAP's solver has a smaller convergence radius than our algorithm. In order to obtain the solution for $Ra = 10^6$, FIDAP has to perform a sequence of solutions for $Ra = 10^3, 10^4, 10^5, 10^6$ and take the solution for lower Ra as the starting value for the solution for higher Ra. Such a solution procedure can become computationally very expensive when the problem size increases, especially in 3D case.

Test Problem 5

As in the first test problem, we consider a closed slot with the $\varepsilon = 0{\cdot}6, A = 10, Pr = 0{\cdot}71$ and $T_r = 300$ K, but with $Ra = 10^5$. A graded mesh of 2160 rectangular elements with 6709 nodes (see Figure 14(b)) is used for the problem.

Based on their numerical results, Chenoweth and Paolucci[5] reported that when the aspect ratio A increases from 7 to 10, the flow regime changes from having a single primary roll at the steady state to having two vortices, one centred at $y = 5{\cdot}5$ and the other at $y = 2{\cdot}5$. However, our numerical results show that up to $A = 10$, although there is a second vortex appearing during the transition to steady state, the flow returned to a steady state with a single primary roll (see Figures 11 and 12). This disagreement between our results and Chenoweth and Paolucci's indicates that the conclusion of such a transition of the flow regime needs more physical proof. Chenoweth and Paolucci's finding may have resulted from the lack of convergence to steady state of their numerical scheme. Their scheme is less implicit in nature than our algorithm and therefore less stable than our scheme in terms of the ability to damp out errors. This may cause the convergence to steady state to be slow or even impossible.

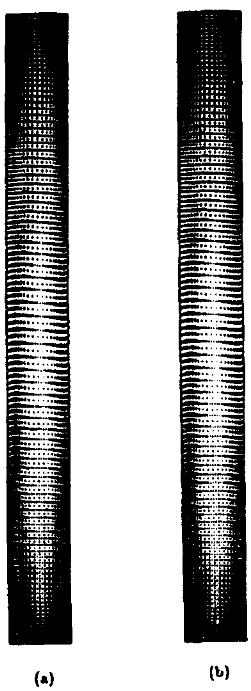

Figure 11. Velocity fields: (a) with correction to p_T^{n+1}; (b) without correction

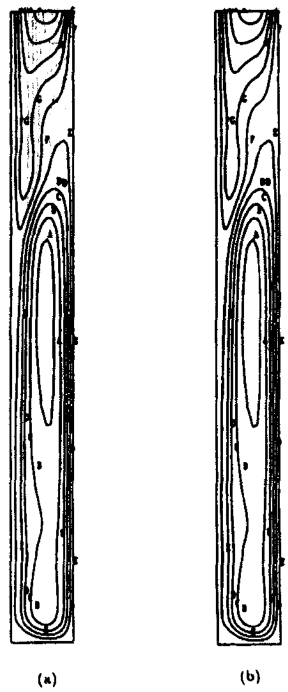

Figure 12. Streamlines: (a) with correction to p_T^{n+1}; (b) without correction

Figures 11(a)–13(a) show the velocity field, streamlines and isotherm field respectively of the solution of our L-model with correction to p_T^{n+1} for global mass conservation and Figures 11(b)–13(b) show the corresponding results without correction. It is clearly seen that the two solutions are almost identical. This again proves that our solution algorithm does not rely on the correction to p_T^{n+1} for global mass balance to maintain solution accuracy. In fact, without correction the deviation from global mass balance is less than 0·35%. Table IV shows that the difference between the two solutions is also less than 0·35%.

8. A BRIEF DISCUSSION ON GLOBAL MASS CONSERVATION

In the case of closed flow, global mass should be conserved. When one adopts the approach of filtering out the acoustic waves by separating the pressure p into a thermodynamic part p_T which is spatially uniform and a hydrodynamic part p_d, the conservation of global mass has always been a concern, because the density calculated from the discrete solution of temperature and p_T does not in general satisfy the constraint of global mass conservation. Some authors, e.g. Chenoweth and Paolucci,[5] use a correction to p_T^{n+1} to maintain the exact global mass balance and hence the accuracy of the discrete solution. However, such a correction is not always feasible or even possible for general flows; in particular, global mass conservation no longer holds in the case of open flows. Algorithms depending on such a correction to maintain solution accuracy cannot be used safely for such general flow problems. For general applications, what we need is an algorithm which does not rely on such a correction but still maintains good solution accuracy for both closed and open flow problems. Our algorithm *is* indeed such a generally applicable algorithm.

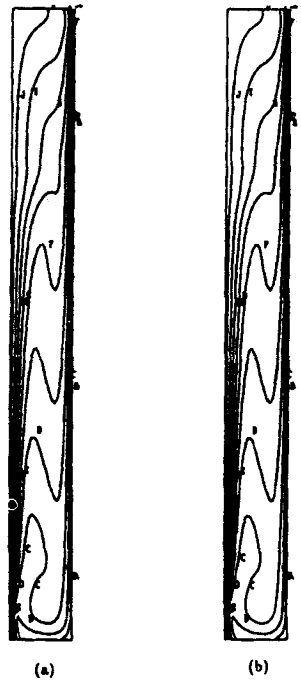

Figure 13. Isotherm fields: (a) with correction to p_T^{n+1}; (b) without correction

A rigorous numerical analysis of our algorithm will be the topic of future papers by the authors. Here we would just point out that, locally, the discrete solution of density by our algorithm is consistent with the continuity equation, or in other words, the discrete density satisfies the continuity equation within the local truncation (or discretization) error of the discrete continuity equation. This consistency and the stability of the algorithm guarantee that the deviation from mass balance is within the discretization error and will not grow and that the discrete solutions will converge to the exact solution when the mesh size and time step size are reduced. Globally, without correlation to p_T^{n+1}, the deviation from global mass conservation satisfies the relation

$$\int_\Omega (\rho^{n+1} - \rho^n)[1 + O(\Delta t)]\,\mathrm{d}\mathbf{x} = 0.$$

Therefore, as long as the time step size Δt is reasonably small, the deviation from global mass conservation is negligible and the accuracy of the solutions will not be affected by this amount of deviation. In fact, for the numerical experiments in the previous section the time step sizes used are

(a) $\Delta t = 1{\cdot}0$ for $A = 10, Ra = 10^3$
(b) $\Delta t = 0{\cdot}2$ for $A = 10, Ra = 10^5$
(c) $\Delta t = 0{\cdot}5$ for $A = 10, Ra = 10^6$

Table IV. Steady state values of p_T and ψ_{max} (maximum value of streamfunction): A-sln.—with correction to p_T^{n+1}; B-sln.—without correction

	A-sln.	B-sln.	Diff. of A, B
p_T	0·9568	0·9538	0·31%
ψ_{max}	0·1476	0·1478	0·14%

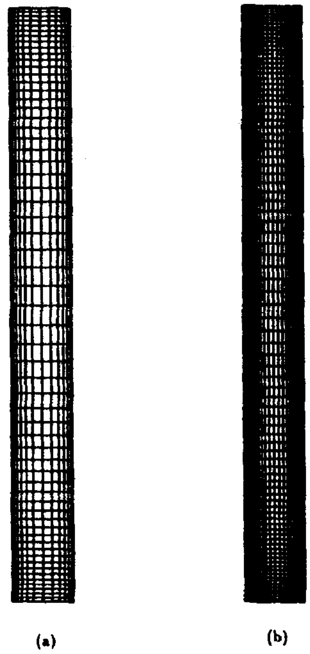

Figure 14. Meshes for $A = 10$: (a) for $Ra = 10^3$; (b) for $Ra = 10^5$

which are not that small at all in practice. The good accuracy of the solutions by our algorithm has been proved by the numerical results in the previous section for both Boussinesq and non-Boussinesq cases.

APPENDIX: NOMENCLATURE

C_p	specific heat when pressure fixed
C_v	specific heat when volume fixed
g	gravity
k	heat conductivity
k_r	reference conductivity
L	reference length
p	pressure
p_d	hydrodynamic part of p
$p_{d,r}$	reference dynamic pressure
p_T	thermodynamic part of p
$p_{T,r}$	$R\rho_r T_r$
Pr	$\mu_r C_p/k_r$, Prandtl number
Q	volumetric heat source
R	$C_p - C_v$, gas constant
T	temperature
T_r	representative temperature
$\mathbf{u}$	velocity vector
U	reference velocity

Greek letters

α_r $k_r/\rho_r C_p$, diffusivity
β_r $1/T_r$, thermal expansion coefficient
γ C_p/C_v, equals 1·4 for air
δT temperature variation scale
μ molecular viscosity
μ_r reference viscosity
ρ density
ρ_r representative density

Miscellaneous

$\mathbf{\nabla}$ gradient operator
$D/Dt = \partial/\partial t + \mathbf{u}\cdot\mathbf{\nabla}$, total time derivative operator
$\mathbf{v}\cdot\mathbf{w}$ scalar product of $\mathbf{v}$ and $\mathbf{w}$

REFERENCES

1. W. Aung, 'Developing laminar free convection between vertical flat plates with asymmetric heating', *Int. J. Heat Mass Transfer*, **15**, 2293–2308 (1972).
2. W. R. Briley, H. McDonald and S. J. Shamroth, 'A low Mach number Euler formulation and application to time-iterative LBI schemes', *AIAA J.*, **21**, 1467–1469 (1983).
3. Y. Horibata, 'Numerical simulation of a low-Mach-number flow with a large temperature variation', *Comput. Fluids*, **21**, 185–200 (1992).
4. C. L. Merkle and Y. H. Choi, 'Computation of low-speed flow with heat addition', *AIAA J.*, **25**, 831–838 (1987).
5. D. R. Chenoweth and S. Paolucci, 'Natural convection in an enclosed vertical air layer with large horizontal temperature differences', *J. Fluid Mech.*, **169**, 173–210 (1986).
6. D. R. Chenoweth and S. Paolucci, 'Gas flow in vertical slots with large horizontal temperature differences', *Phys. Fluids*, **28**, 2365–2374 (1985).
7. G. de Vahl Davis, 'Natural convection in a square cavity—a bench mark solution', *Int. j. numer. methods fluids*, **3**, 249–264 (1983).
8. E. Dean, R. Glowinski and C. H. Li, 'Application of operator splitting methods to the numerical solution of nonlinear problems in continuum mechanics and physics', in J. Goldstein, S. Rosecrans and G. Sod (eds) *Mathematics Applied to Science*, 1988.
9. E. Dean, R. Glowinski and C. H. Li, 'Supercomputer solutions of partial differential equation problems in computational fluid dynamics in control', *Comput. Phys. Commun.*, **53**, 401–439 (1989).
10. C. H. Li, 'Numerical solution of Navier–Stokes equation by operator splitting', *Proc. Sixth Int. Conf. in Australia on Finite Element Methods*, Vol. 1, 1991, pp. 205–214.
11. C. H. Li, 'Numerical simulation of flow past a circular cylinder by operator splitting, *Tech. Rep. DMS-C 91/11*, 1991.
12. C. H. Li, 'On the numerical simulation of incompressible viscous flow by operator splitting', *Tech. Rep. DMS-C 91/12, 1991.*
13. D. D. Gray and A. Giorgini, 'The validity of the Boussinesq approximation for liquid and gases', *Int. J. Heat Mass Transfer*, **19**, 545–551 (1976).
14. D. K. Gartling and C. B. Hickox, 'A numerical study of the applicability of the Boussinesq approximation for a fluid saturated porous medium', *Int. j. numer. methods fluids*, **5**, 995–1013 (1985).